J Nanopart Res (2024) 26:4
https://doi.org/10.1007/s11051-023-05904-1

RESEARCH PAPER

Rapid removal of methylene blue and tetracycline by rough particles decorated with Pt nanoparticles

Faizan Khan · Chandra Shekhar · Tarak Mondal · Manigandan Sabapathy

Received: 17 January 2023 / Accepted: 26 November 2023

Abstract The increasing groundwater pollution resulting from industrial dyes and pharmaceutical products, which come from various sources, requires urgent attention to implement effective remediation measures. We demonstrate that the rough particles studded with platinum (Pt) nanoparticles can be fabricated at room temperature straightforwardly and in a single step. These rough particles displayed a good catalytic power (100% removal efficiency) against a model industrial dye (methylene blue) and pharmaceutical residue (tetracycline) within a reasonable time scale. Characterization techniques such as X-ray diffraction (XRD), atomic force microscopy (AFM), and field emission scanning electron microscopy (FESEM) confirmed the uniform deposition of Pt nanoparticles on the surface of polystyrene particles, forming dense islands and the roughened surface. Further, we investigated the influence of particle size, concentration, and contact patterns on the performance of rough catalytic particles. The semi-batch conditions favoured the complete decomposition of tetracycline within 40 min, but the batch-wise operation offered a good contacting pattern for methylene blue, yielding a maximal output within 10 min. The kinetics of the heterogeneous catalytic process modelled by Langmuir-Hinshelwood kinetics ($r = k_r KC/1 + KC$) predicts that the given methylene blue decomposition reaction induced by the rough particles follows the pseudo-first-order kinetics. The rate constants for the reaction catalyzed by 0.6 and 1.0 μm-sized rough particles are 0.048 and 0.032 min^{-1}, respectively. Furthermore, we established the proof-of-concept using magnetically responsive nanoparticles for real-time applications, including decontamination and recovery of catalyst particles via an externally applied magnetic field in one cycle. Our proposed method helps achieve a near-100% degrading efficiency within 10 to 40 min at minimal catalytic particle concentration, i.e., 200 ppm. Since we can turn the rough particles into super-paramagnetic, we can recover and reuse them for several wastewater treatment cycles without incurring running costs.

Keywords Polystyrene (PS) · Iron Oxide (IO) · Platinum nanoparticles · Rough particles · Magnetically-responsive nanoparticles · Methylene blue · Tetracycline · Environmental remediation

1 Introduction

The rapid rise of contamination in the groundwater due to industrial dyes and pharmaceutical products generated from textile and pharma industries has been a most

Faizan Khan and Chandra Shekhar contributed equally to this work.

Supplementary Information The online version contains supplementary material available at https://doi.org/10.1007/s11051-023-05904-1.

M. Sabapathy (✉) · F. Khan · C. Shekhar · T. Mondal
Department of Chemical Engineering, Indian Institute of Technology Ropar, Rupnagar 140001, Punjab, India

Published online: 21 December 2023

pressing issue globally that it has urged the intervention of policymakers, researchers, and engineers around the globe [1,2]. Although the contamination of several azo-based dyes and pharmaceutical residues is a matter of concern, the primary issue that remains to be tackled is the establishment of efficient removal of the contaminants from wastewater as they pose a severe threat to the ecology. In recent years, much attention has been given to the advanced oxidation processes (AOPs) over traditional water treatment methods such as mechanical separation, coagulation, and filtration. The various techniques of AOPs include (1) photolysis [3,4], (2) Fenton reaction [5,6], (3) photo-Fenton [6,7], (4) photocatalysis [3,8–10], (5) ozonation [8,11], (6) sonochemistry [6,12], (7) adsorption [13–17], and (8) microwave [18–22]. Despite the advancement in these techniques being well received under AOPs, each method has merits and demerits. For instance, high energy demand (sono), strict pH range (Fenton) [23], high H_2O_2 consumption (Fenton/photo-Fenton), and cost of implementation.

Among several AOPs, Fenton reaction-based methods are found to be the most efficient for removing organic pollutants [24]. Nevertheless, this method is not attractive due to shortcomings, such as (1) the tendency to aggregate and sediment against gravity, (2) process conditions that demand a narrow pH range of 2–3 to be maintained, and (3) high peroxide consumption. On the contrary, heterogeneous Fenton-like catalyst-assisted reaction based on iron oxides [24], transition metal oxides [25], and the alloy made up of zero-charge metal/metal-iron oxides [26] are promising candidates owing to its increased electrocatalytic activity even at higher pH. Toda et al. reported the enhanced electrocatalytic activity of Pt alloyed with Fe electrodes. Based on the analysis by these authors, the enhanced electrocatalytic activity is due to increased d-electron vacancy of the Pt surface induced by alloying the metal with Fe [27]. Furthermore, the efficiency of the Fenton reaction (based on Fe_3O_4 nanoparticles) is expected to decrease as the considerable amount of hydroxyl and perhydroxyl radicals formed during reaction are involved in converting Fe^{3+} back to Fe^{2+}, in addition to organic molecules. However, the decomposition reaction catalyzed by platinum-x hybrid particles instead of Fenton eliminates the perhydroxyl formation, and the unwanted reaction step [5]. In 2012, Hsieh and Lin reported the electrocatalytic activity of Fe-Pt nanoparticles (Fenton-like) for the first time with a maximum efficiency of 90% by the end of the 90 min reaction time [5]. The study of the decomposition of MB based on the Pt/Fe route was not pursued by many researchers considering the cost of synthesis involved, despite knowing the fact that the issue associated with the cost of production could be eliminated by employing a magnetically responsive core-shell particle system decorated with platinum nanoparticles, as the particles can be recovered by applying magnetic force externally. Such particles are regarded as rough particles with controlled surface deposition. We aim to demonstrate the chemical decomposition of MB (an example system of azo dyes) and tetracycline (an example system of pharmaceutical drugs) using nano and micron-sized polystyrene (PS) rough particles decorated with platinum as a catalyst. Since the organics mentioned above are chemically deactivated, there is no need to regenerate the catalyst particles once the reaction is completed. Furthermore, since the particles can be made magnetically responsive and easily separated by applying magnetic force externally, it is possible to carry out the treatment process continuously with less or no manual intervention without regeneration. Thus, as outlined above, the method of heterogeneous catalyst particles is a cost-effective alternative, as the costs spent are predominantly linked to the capital budget or one-time investment.

In the context of the synthesis of rough particles concerning immobilization of metallic nanoparticles, a common approach has been to decorate the surface of core particles with gold (Au) or any other metallic nanoparticles via electrostatic interaction, or covalent bonding [28–32]. These routes demand that the core particles be cationic to adsorb/deposit the gold nanoparticles (anionic) to make suitable rough colloids. However, it is of interest to immobilize platinum (Pt) instead of Au nanoparticles to explore its application in the field of contaminant removal. The synthesis route follows the covalent bonding route in which the Pt nanoparticles are deposited by the chemical reduction of platinic acid using a reducing agent such as sodium borohydride ($NaBH_4$). In 2012, Hsieh and Lin devised Fe-Pt nanoparticles to deactivate MB dye to achieve a more significant reaction extent [5]. However, the method offered by Hsieh and Lin is slightly complicated and involves heating to 297°C. Therefore, it is essential to study heterogeneous catalysts of many kinds to find the suitability of the method to tackle various pollutants. Thus, we have chosen to extend the studies beyond Fe-

based supports to get insight into the degradation kinetics against other organics removal. For instance, the as-synthesized Pt-based rough particles have shown good catalytic activity in decomposing hydrogen peroxide, which helps degrade methylene blue (MB) and tetracycline (TC). Our suggested technique achieves a near-100% degrading efficiency within 10 to 40 minutes at lower concentrations (200 ppm), making it a viable alternative to Fenton-based AOPs.

The remainder of the manuscript is structured as follows: To provide the reader with a better understanding, we first address the synthesis, characterization, and application of Pt-decorated PS rough particles for wastewater treatment. Consequently, we show the proof-of-concept (POC) by using magnetically responsive rough nanoparticles (MR-RP) for the application. In addition to the application of discolouration or deactivation, this POC portion addresses the separation of catalyst particles under an externally applied magnetic force.

2 Experimental

2.1 Materials

We used Invitrogen™ grade amidine functionalized polystyrene (PS) latex particles purchased from Thermo Fisher Scientific, India, to prepare catalytic-enabled rough particles for treating the wastewater containing specific contaminants. The particles of this type with different sizes were employed for the decomposition reaction. The size of the particles employed, as per the manufacturer's specifications, are 1.0, 0.5, and 0.02 μm. However, the size of the particles determined based on image analysis using a scanning electron microscope (SEM) and dynamic light scattering (DLS) technique are 1.0 $\pm$ 0.1, 0.579 $\pm$ 0.006, and 0.022 $\pm$ 0.001 μm. An electrophoretic study was conducted to determine the particles' potential at the boundary between the shear and diffuse plane, i.e., Zeta potential (ζ). The ζ potential of the particles determined for PS particles of size 1.0, 0.6 (rounded-off), and 0.02 μm in 1 mM NaCl electrolyte medium were 46 $\pm$ 3, 55.8 $\pm$ 3.2, and 42.7 $\pm$ 1 mV, respectively. To prepare a core-shell assembly of magnetically responsive rough particles, we employed iron oxide (IO) nanoparticles purchased from Sigma Aldrich Chemicals Pvt. Ltd., India. Polydiallyldimethylammonium chloride (DADMAC), gifted by Dr. Sarang Gumfekar, IIT Ropar, was used to modify the IO particles by imparting positive sites to the surface. Chloroplatinic acid hexahydrate ($H_2PtCl_6.6H_2O$), used as precursor solution to deposit platinum (Pt) nanoparticles on the PS surface, was procured from Sigma-Aldrich Chemicals Pvt. Ltd., India. Sodium borohydride ($NaBH_4$), obtained from Sigma-Aldrich Chemicals Pvt. Ltd., was used as a reducing agent. Hydrogen peroxide (30 w/v %), used in the decomposition reaction mixture to generate hydroxy radical, was procured from Sigma-Aldrich Chemicals Pvt. Ltd., India. The model pollutants used to demonstrate the deactivation kinetics, such as methylene blue and tetracycline, were procured from Sigma-Aldrich Chemicals Pvt. Ltd., India. A hydrogen peroxide test strip (MQuant® Peroxide-Test) received from Sigma-Aldrich Chemicals Pvt. Ltd., India, was used to quantitatively predict the catalytic-assisted decomposition kinetics under the presence of rough colloids. All reagents received were analytical grades and used without any further purification. The deionized water obtained from a Smart2Pure™ water purification system (Make: Thermo Fisher Scientific, Model: Smart2Pure 12 UV/UF) was used for all experiments involving the use of aqueous solutions.

2.2 Synthesis of PS rough particles decorated with Pt

First, we prepared a chloroplatinic acid hexahydrate solution using DI water such that the precursor concentration in the stock solution was 10 mM. We devised a wet-chemical method to achieve a uniform deposition of Pt nanoparticles on the PS surface in an endless array of monolayer fashion. The deposition of Pt nanoparticles was realized using the method reported by our group that involves the deposition of gold (Au) nanoparticles [33]. However, a slightly different strategy was used, including a wet-chemical deposition by nucleating Pt nanoparticles instead of Au on the PS surface. Since both the precursors of Au and Pt bear a net negative charge, favouring the attachment of ions over the positive sites of PS due to net electrostatic attraction, the modified protocol helped us synthesize Pt-decorated PS particles in a single step. Unlike the work of Lu et al., our modified protocol is devoid of pre-deposition of Au nanoparticles as seeds to catalyze the reduction reaction of $PtCl_6^{2-}$ ions [34]. Figure 1 depicts the schematic description of making rough particles

Table 1 Average size and zeta potential of the PS and IO particles

Type	Avg. Size (μm)	Zeta potential (mV)	
		Bare	Modified
PS	0.02 ± 0.009	42.7 ± 1.0	-33 ± 0.7
	0.6 ± 0.006	55.8 ± 3.2	-33 ± 0.3
	1.0 ± 0.1	46 ± 3	-35 ± 0.4
IO	0.06 ± 0.001	-2.7 ± 1.8	33.2 ± 2.2

and their application towards wastewater treatment. As explained in Fig. 1A, a known concentration of platinum precursor (0.5 mM), PS particles (0.5 mg/mL) are mixed using a magnetic stirrer for up to 30 min before adding a reducing agent, sodium borohydride, to the mixture. Subsequently, after the equilibration of the mixture for about 30 min, the chemical reduction reaction is induced by adding 5 mL of 10 mM sodium borohydride solution into the beaker containing the reaction mixture. The reaction is allowed to continue until the solution becomes clear. To achieve maximum conversion, an excess of sodium borohydride has been employed, specifically ten-fold. Additionally, we have given sufficient time for reaction, i.e., 4 h. Note: The reaction mixture becomes transparent and clear when the chemical reduction process continues for up to four hours. Further, these samples were allowed to undergo centrifugation to separate the modified PS particles by removing the supernatant and washing them several times. The particles recovered in this way are further utilized to study the kinetics of MB and TC decomposition. Table 1 presents the size and zeta potential (ζ) of the bare PS and the rough PS particles. The negative ζ values of Pt-deposited PS particles are attributed to the adsorption of borohydride or borohydride derivatives on the surface of Pt. Many researchers have reported the effect of reducing agents on the zeta potential values of metallic colloids such as gold nanoparticles [35,36]. Karimi et al. reported that the zeta potential values of gold nanoparticles produced with sodium borohydride are higher than sodium citrate [35].

2.3 Selection of target pollutants

Two representative pollutants from the family of azo dyes and antibiotic drugs, such as MB and TC, were chosen for the decomposition studies. We endeavoured to understand the role of rough particles in the chemical deactivation of these target pollutants. The initial pollutants concentration was maintained constant at 15 μM throughout while the decomposition of the respective pollutants was studied in batch and semi-batch conditions to replicate the real-time process of large-scale operation.

2.4 Heterogeneous batch degradation process

All degradation experiments that involve batch-wise operations were performed in different initial volumes, such as 25, 50, and 100 mL. The rough particle concentrations employed were 200, 100, and 50 ppm, respectively. For the studies, we prepare the required mixture using the rough particles at appropriate concentrations along with the target pollutants with known initial concentration, i.e., 15 μM, to induce the decomposition reaction in the presence of a known amount of H_2O_2, 5 vol% per the total volume mentioned above. The reaction is set to proceed for the desired time by adding the radical generator, i.e., H_2O_2. Further, the reaction mixture is continuously stirred using a stirrer at a programmed speed of 140 RPM. The entire reaction was conducted at room temperature, 25°C, throughout the desired duration.

2.5 Heterogeneous semi-batch degradation process

All degradation experiments that involved semi-batch operations were performed in different initial dosing volumes at a uniform interval of 10 min until completion. The rough particle concentrations employed were 200, 100, and 50 PPM, respectively. For the studies, we prepare the required mixture using the rough particles at appropriate concentrations along with the target pollutants with known initial concentration, i.e., 15 μM, to induce the decomposition reaction in the presence of a known amount of H_2O_2, 5 vol% per the total initial volume. The reaction is initiated to proceed for the desired length by adding the radical generator, i.e., H_2O_2 at a desired dosing volume. Using the stirrer, we stirred the reaction mixture nonstop at a programmed speed of 140 RPM. The decomposition reaction was conducted at room temperature, 25°C, throughout the desired duration.

Figure 1B and E depict the schematic description showing the catalytic action of PS rough particles and

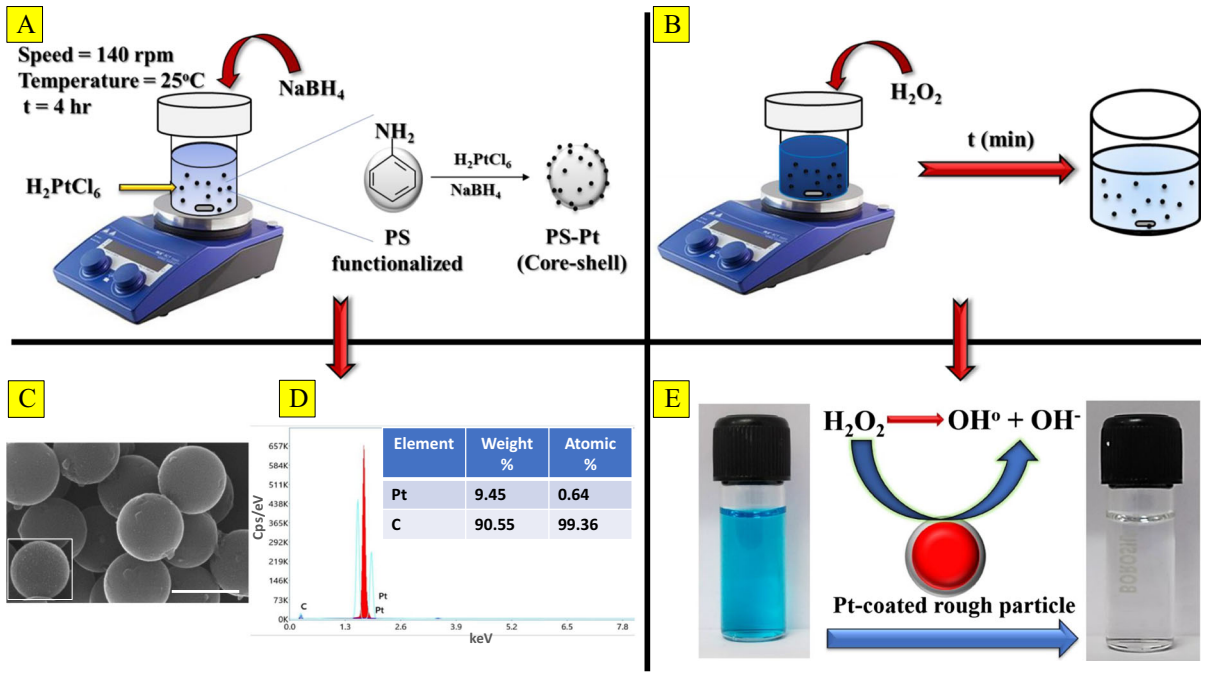

Fig. 1 Schematic description showing the process of synthesizing rough particles and their application towards deactivation of the target pollutants. **A** Schematic illustration showing the synthesis methodology of making rough particles. **B** Schematic illustration showing the application of rough particles in treating wastewater containing the target pollutants. **C** and **D** FESEM and EDX spectrum of 0.6 μm rough particles modified with Pt nanoparticles, respectively. **E** Vial pictures showing the discoloration of MB dye in the presence of rough particles

the discolouration process of MB due to contact with the modified PS particles of varying sizes, respectively.

2.6 Hydrogen peroxide decomposition

To understand the kinetics of H_2O_2 decomposition, we decoupled the decomposition reactions of MB and TC by eliminating them in the lab-scale reactor. Subsequently, in a separate set of experimental studies, the reaction flasks containing H_2O_2 and rough particles were employed to conduct investigations at different lengths of time. We recorded the concentration vs time of H_2O_2 as the reaction proceeds to understand the effect of contacting patterns on the catalyst-assisted H_2O_2 decomposition reaction.

2.7 Characterization

The zeta potential of bare PS and rough PS particles were measured based on the electrophoretic light scattering (ELS) technique using Zetasizer procured from Malvern Instruments, Model: Zetasizer Nano ZSP. The average diameter of PS particles of 0.6 μm and 1.0 μm were determined using a high-resolution scanning electron microscope (HRSEM), Make: FEI, USA and Model: Inspect F. The hydrodynamic radius of PS of size 22 nm was deduced using the dynamic light scattering (DLS), Make: Malvern Instruments, and Model: Zetasizer Nano ZSP. To confirm the distribution of platinum (Pt) particles on the surface of core polystyrene (PS) particles, the atomic force microscopy (AFM) (Make: Bruker Corp. Germany, Model: Multimode-8 AFM) and electron mapping analysis using a scanning electron microscope (Make: JEOL Ltd. Japan, Model: JSM-6610) were conducted on the as-synthesized rough particles engineered with Pt nanoparticles. The kinetics of MB and TC decomposition reactions were studied by capturing concentration as a function of time using UV–VIS spectrophotometers (Make: Hach company US, Model: DR3900 & Make: PerkinElmer Inc., USA, Model: LAMBDA

365). The surface area of the platinum-coated particles was determined using BET analysis (Make: Microtrac BEL Corp. Japan, Model: BELSORP Max II). X-ray diffraction (XRD), Make: Bruker Corp. Germany, Model: Bruker D8 Venture, was utilized to analyze the PS particles and platinum-coated PS rough particles to gain a deeper understanding of their properties in their as-synthesized state. To identify any intermediate products formed during the decomposition of TC and MB, the LC-MS/MS (Make: Waters Corp. USA, Model: XEVO G2-XS QTOF) technique was performed using a C18 column with Triple Quad, utilizing H_2O and acetonitrile with 0.1% (v/v) formic acid solution as mobile phases at room temperature with a flow rate of 4 ml/min and 2 μL injection rate.

3 Results and discussion

3.1 Characterization of rough particles

FESEM was used to determine the size of PS particles and the morphological changes in PS rough particles due to the reaction. EDX was performed concurrently to identify the presence of Pt nanoparticles. Figure 2 displays the surface morphology of surface-engineered PS rough particles decorated with Pt nanoparticles in the form of islands (Fig. 2A and B) and the EDX spectrum used to validate the deposition of Pt nanoparticles on the surface of PS (Fig. 2C and D). As depicted in Fig. 2C and D, the distinctive peaks at 1.5 KeV indicate the existence of Pt nanoparticles. To confirm

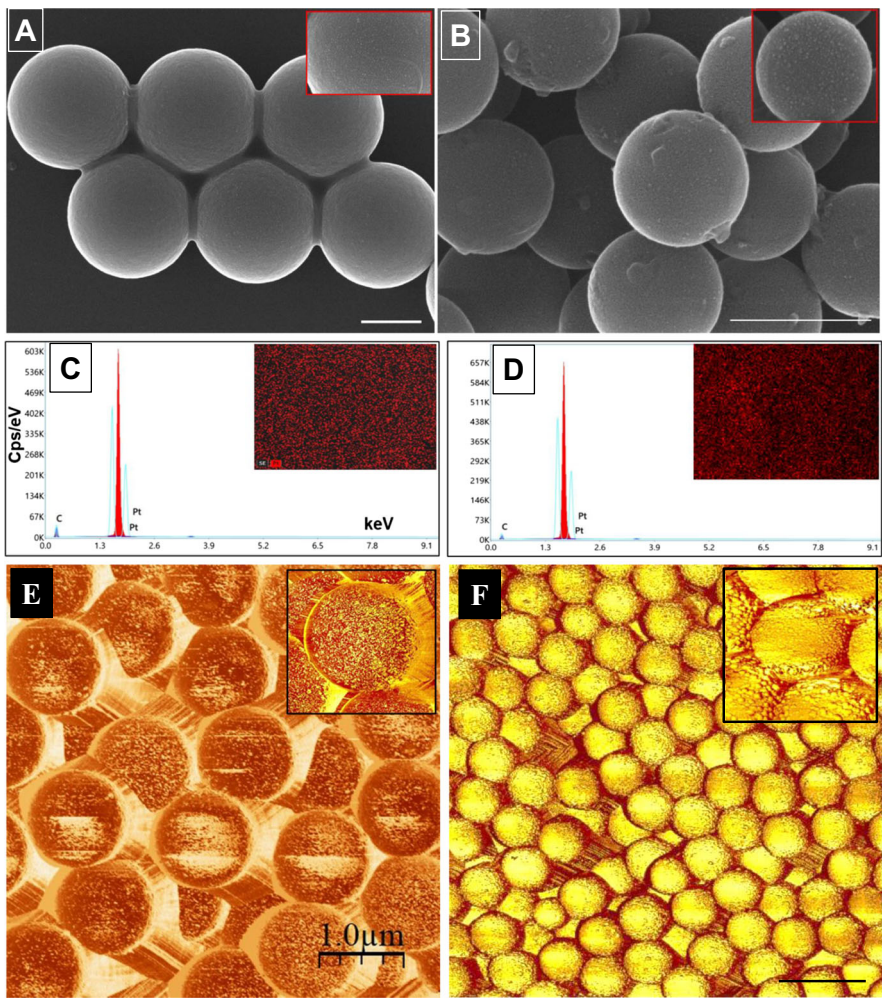

Fig. 2 Structural characterization of modified PS particles. **A** and **B** FESEM images of 1.0 and 0.6 μm, respectively. **C** and **D** EDX spectrum of 1.0 and 0.6 μm, respectively. **E** and **F** AFM images of platinum-deposited PS particles of sizes 1.0 and 0.6 μm, respectively. The scale bars given in the FESEM images correspond to 500 nm. The scale bar given in Figure 2F (AFM) corresponds to 1.0 µm

the distribution of platinum (Pt) particles on the surface of core polystyrene (PS) particles, we utilized AFM and electron mapping analysis on the synthesized rough particles engineered with Pt nanoparticles. In Fig. 2C, D, E, and F, we present the AFM images and electron mapping of the rough particles, which demonstrate the deposition of Pt in the form of islands. These findings suggest that the Pt nanoparticles are uniformly distributed throughout the surface of the larger PS particles. In the case of electron mapping, the red spots in the images confirm the uniform distribution of Pt nanoparticles in the matrix throughout. High-resolution atomic force microscopy provides a clear contrast between metal and polymer boundaries, confirming the existence of metallic nanoparticles as uniformly distributed denser islands. Further, a line-cut analysis has been performed to examine the morphological distinctions between bare and rough particles. In short, atomic force microscopy (AFM) has collected surface attributes and interactions. The force-distance measurements, involving the indentation and retraction of force, were employed to quantify the adherence of platinum nanoparticles onto rough surfaces and illustrate the deposition of Pt in the form of islands on the surface of polystyrene (PS) particles. Figure 3 A and B represent 1 μm bare and rough particles. Similarly, Fig. 3C and D depict the surface profile of bare and rough particles of size 0.6 μm, respectively. The surface roughness data (Fig. 3B and D) suggest that Pt nanoparticles are evenly distributed across the surface of the larger PS particles as islands.

Figure 4 illustrates the X-ray diffraction pattern obtained from the particles, and the presence of platinum nanoparticles was detected at angles of 39.81°, 46.31°, and 67.61°, confirming the 110, 200, 220 orientation, respectively. These findings align with previously reported results in the literature [37]. Further, the surface area of the platinum-coated particles exposed to hydrogen peroxide was determined using BET analysis. The results revealed that particles with sizes of 0.02 μm and 1 μm had specific surface areas of 6.83×10^1 m^2/g and 6.63 m^2/g, respectively. While we initially assumed that nanoparticles would have a larger surface area than microparticles, they demonstrated reduced

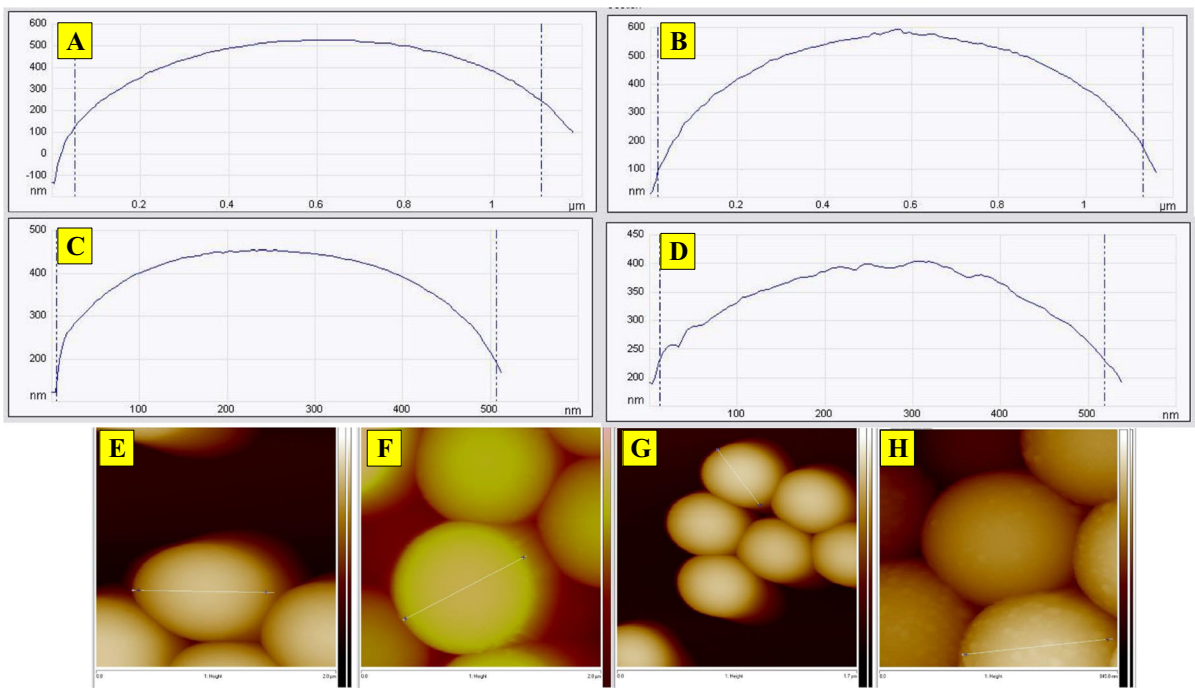

Fig. 3 Line-cut analysis of bare and rough particles using AFM technique: **A** and **B** show the line-cut analysis for the bare and rough particles of size 1 μm, respectively, and **C** and **D** show the line-cut analysis for the bare and rough particles of size 0.6 μm, respectively. **E** and **F** AFM images of the bare and rough particles of size 1 μm, respectively, showing the surface line. G and H) AFM images of the bare and rough particles of size 0.6 μm, respectively, showing the surface line

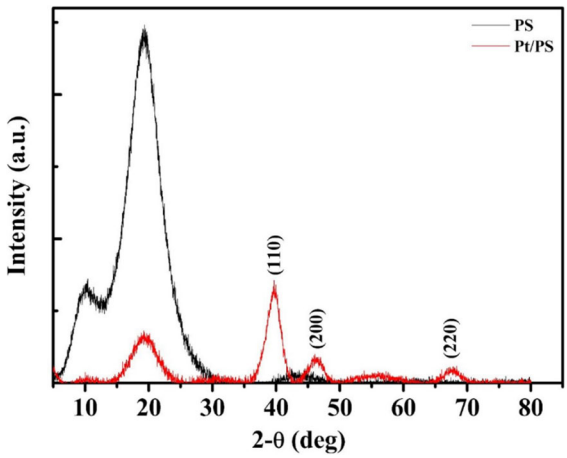

Fig. 4 XRD spectrum showing the characteristic peaks corresponding to bare (PS) and rough particles (Pt/PS) of size 1.0 μm

catalytic activity due to buoyancy effects arising from bubble formation during hydrogen peroxide decomposition, the details of which are provided in the later part of this manuscript.

3.2 Batch and semi-batch experiments

Next, we discuss the performance of rough particles in batch and semi-batch conditions. This study highlights the engineering processes that can substantially impact transitioning between real-time applications. Figure 5 refers to the decomposition reaction catalyzed by rough particles (Pt/PS) in the presence of a moderate concentration of 5% H_2O_2. Note: The absorbance maxima at 358 nm from each UV–Vis spectral plot were utilized to determine the concentration as a function of time. The concentration of particles and the pollutants used for the comparison study are 100 ppm and 15 μM, respectively. According to the data, the highest TC elimination may be accomplished when the reaction is conducted under semi-batch conditions. On the other hand, when similar decomposition kinetics was run under batch circumstances, the catalyst-assisted heterogeneous response produced a high reaction rate for MB removal, i.e., 100% elimination of MB in 10 minutes. These results intrigued us to set up reaction conditions appropriately. We, therefore, systematically conducted the heterogeneous catalyst-assisted reactions using the rough particles of desired sizes and concentrations.

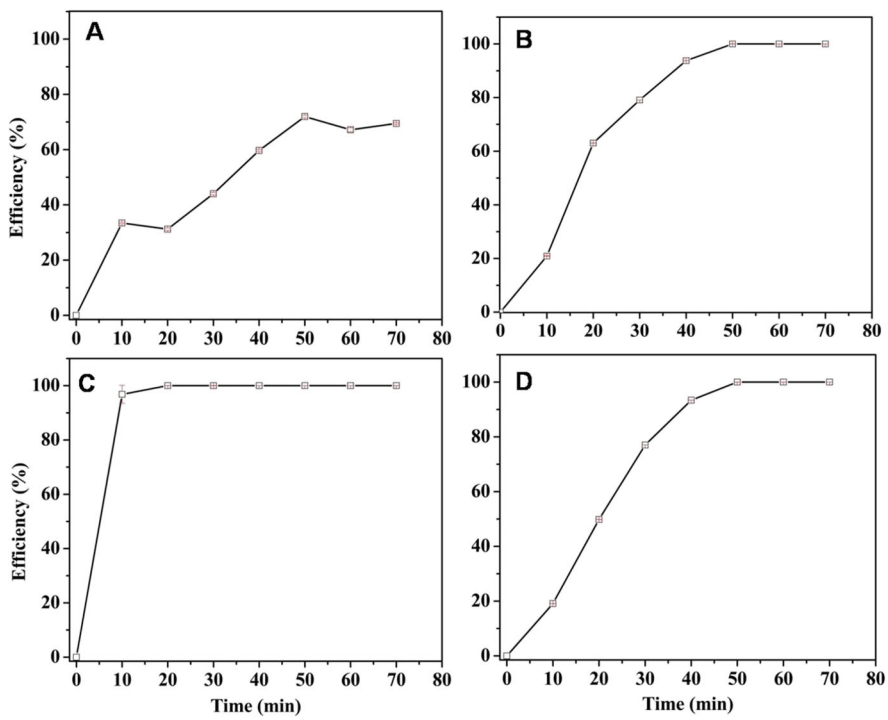

Fig. 5 Decomposition of TC and MB with time. Removal of TC when carried out in batch (**A**) and semi-batch (**B**) set-up. Removal of MB when carried out in batch (**C**) and semi-batch (**D**) set-up. The concentration of rough particles, MB, TC, and H_2O_2 employed are 100 ppm, 15 μM, 15 μM, and 5%, respectively

To this end, we demonstrate the performance of rough particles in semi-batch conditions to determine the optimum parameters. Since the semi-batch operation was effective for TC, we conducted all experiments related to TC removal using a semi-batch set-up to find the optimal point. Figure 6 displays the kinetics of the decomposition reaction of TC carried out in semi-batch operation. By comparing Figs. 5 and 6, the kinetic data suggest that pollutants' concentration has an inverse effect on the reaction rate associated with TC removal. Therefore, the semi-batch catalyzed reaction favours maximal elimination at a higher rate. In contrast to batch mode, this condition improved the reaction rate because H_2O_2 concentrations were kept as low as possible due to drop-wise addition. We infer from Fig. 6 that the maximum efficiency is proportional to particle concentration. Table 2 summarizes the performance of rough particles employed to deactivate TC. As shown in Fig. 6 and Table 2, the rough particles with a size of 0.6 μm and concentration 200 ppm along with a dosing volume of 0.416 mL H_2O_2 exhibited the best performance among the given set of rough particles and the experimental conditions.

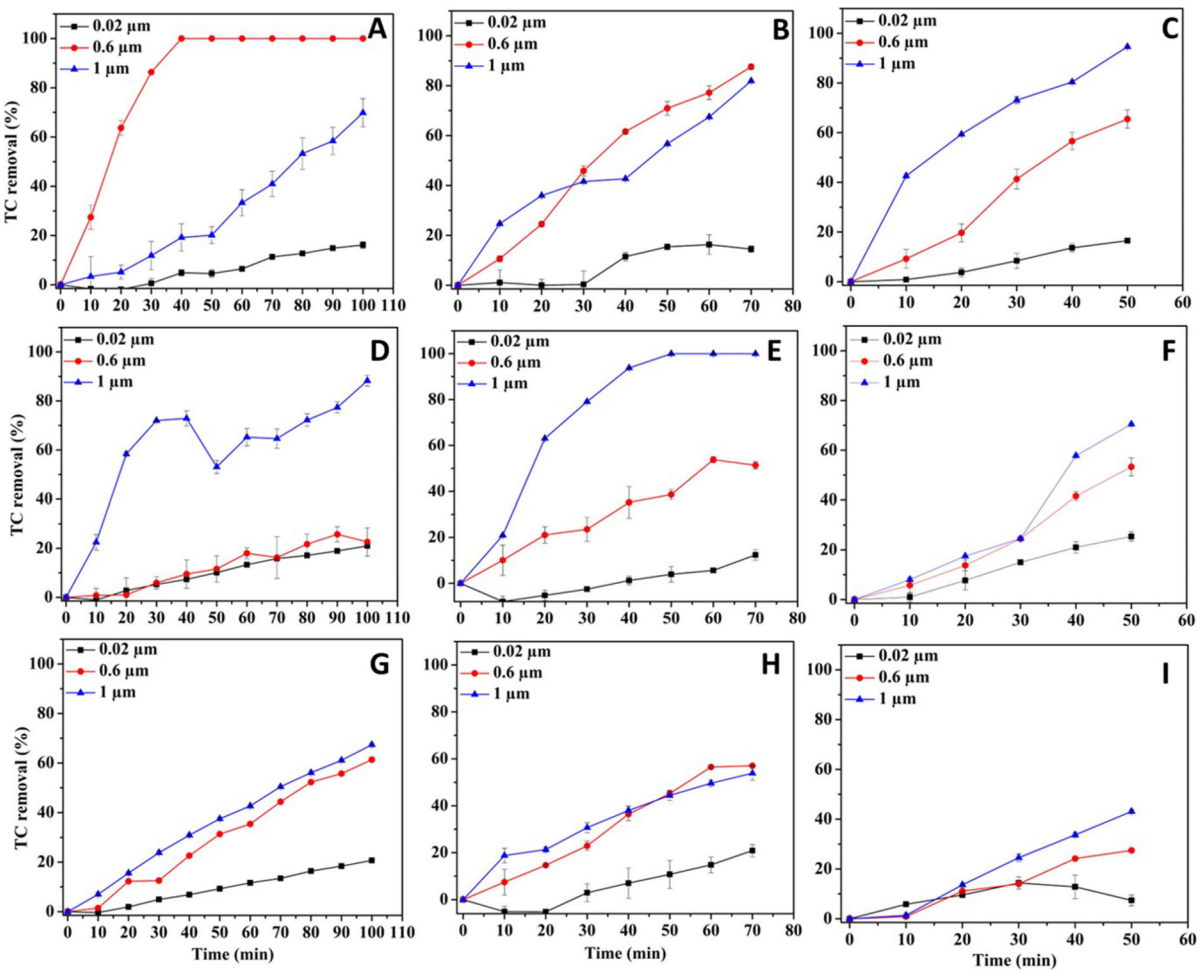

Fig. 6 Effect of dosing volumes of H_2O_2 on the decomposition of TC with time under semi-batch mode at regular intervals. **A–C** Removal of TC at different dosing volumes of 0.416, 0.624, and 0.833 mL of H_2O_2, respectively. **D–F** Removal of TC at different dosing volumes of 0.833, 1.25, and 1.66 mL of H_2O_2, respectively. **G–I** Removal of TC at different dosing volumes of 1.66, 2.5, and 3.33 mL of H_2O_2, respectively. The concentration of rough particles used are 200 ppm (**A–C**), 100 ppm (**D–F**), and 50 ppm (**G–I**), respectively. The initial concentration of TC employed for the study is 15 μM, throughout

Table 2 Summary of performances of the rough particles over the removal of TC

Type	Size (μm)	Initial TC conc. (μM)	Particles conc. (ppm)	Dosing volume (mL)	Max. Efficiency (%)	Time (min)
Pt-PS	1	15	100	1.25	100	50
	0.6		200	0.416	100	40
	0.02		100	1.66	21	50

Further, we discuss the performance of rough particles in batch conditions. Since the batch operation was effective for MB, we ran all experiments related to MB removal using a batch mode to determine the optimal point. Figure 7 displays the kinetics of the decomposition reaction of MB carried out in batch operation. Note: The absorbance maxima at 664 nm from each UV–Vis spectral plot were utilized to determine the concentration as a function of time. We infer that the performances of the rough particles of size 1.0 and 0.6 μm overlap significantly over time. Barring 0.02 μm, the rate of decomposition data shows direct dependency on the concentration of rough particles. Therefore, the batch-catalyzed reaction favours the maximal elimination rate at a higher concentration of rough particles. In contrast to the semi-batch mode, this condition improved the reaction rate because the concentration of H_2O_2 was kept high at the start. Table 3 summarizes the performance of rough particles employed to deactivate MB. As shown in Fig. 7 and Table 3, the rough particles with a size of 1 and 0.6 μm and concentration 200 ppm at a concentration of 5% H_2O_2 exhibited the best performance among the given set of rough particles and the experimental conditions.

Further, the treated water was tested for its chemical oxygen demand (COD) using the standard titration method outlined in the Indian Government's IS3025:2006 standard. The results showed that the COD values of the treated water were within the permissible limit (250 mg/L) for effluent water. The total organic carbon (TOC) corresponding to the treated wastewater was estimated using the equation proposed by Dubber and Gray [38], based on the measured COD values. The estimated TOC values for the treated water samples involving TC and MB using 1.0 μm-sized rough particles were 29.68 mg/L and 31.02 mg/L, respectively. It is worth noting that 1.0 μm-sized rough particles were chosen for the study as they showed 100% removal efficiency in both semi-batch and batch conditions at a concentration of 100 ppm.

3.3 The proposed pathway of TC and MB degradation

In addition to the TOC analysis, an LC-MS/MS technique was used to examine the intermediate products formed during the Fenton-like reaction. The rough particles of size 1.0 μm at a concentration of 100 ppm were employed under semi-batch and batch conditions to find TC and MB degradation products. The reaction time maintained for the analysis of byproducts formation corresponding to MB and TC is 20 and 70 min, respectively. As can be inferred from the proposed degradation scheme, the tetracycline is represented by

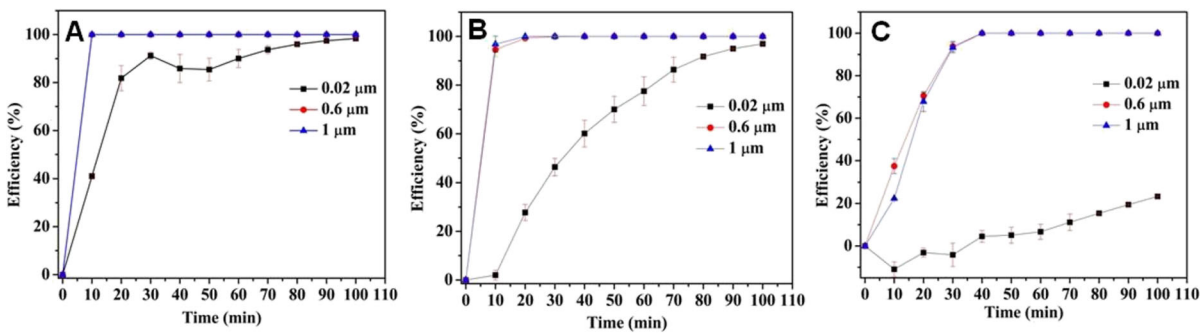

Fig. 7 Removal of MB catalyzed by varying sizes of rough particles at a concentration of **A** 200 ppm, **B** 100 ppm, and **C** 50 ppm

Table 3 Summary of performances of rough particles against MB removal at 5% H_2O_2

Type	Size (μm)	Initial MB conc. (μM)	Particle conc. (ppm)	Max. Efficiency (%)	Time (min)
PS	1 & 0.6	15	200	100	10
			100	100	20
			50	100	40

the 445 m/z, while the mass divided by the charge number associated with MB is 284 m/z. Following a Fenton-like reaction, LC-MS/MS identified four major intermediates in the TC deteriorated solution with masses of 318, 274, 225, and 194 m/z. The suggested intermediates and the ratio m/z obtained from the LC-MS/MS spectra following 70 minutes of TC degradation are shown in Fig. 8A. The loss of the dimethylamino group and dehydroxylation reaction caused the TC to form an intermediate product identified as 318 m/z (product I) [39,40]. Subsequently, the deacetylation combined with oxidation reactions led to the conversion of the product I into product II (274 m/z) and product III (225 m/z) [39]. Finally, the attack of radicals on product III resulted in the formation of yet another intermediate, i.e., product IV, at 194 m/z [40], before being converted into water, carbon-di-oxide, and N-minerals. According to Fig. 8B, a major intermediate product has been observed at 274, as shown in the proposed pathway, due to the addition of °OH and loss of a methyl group [41].

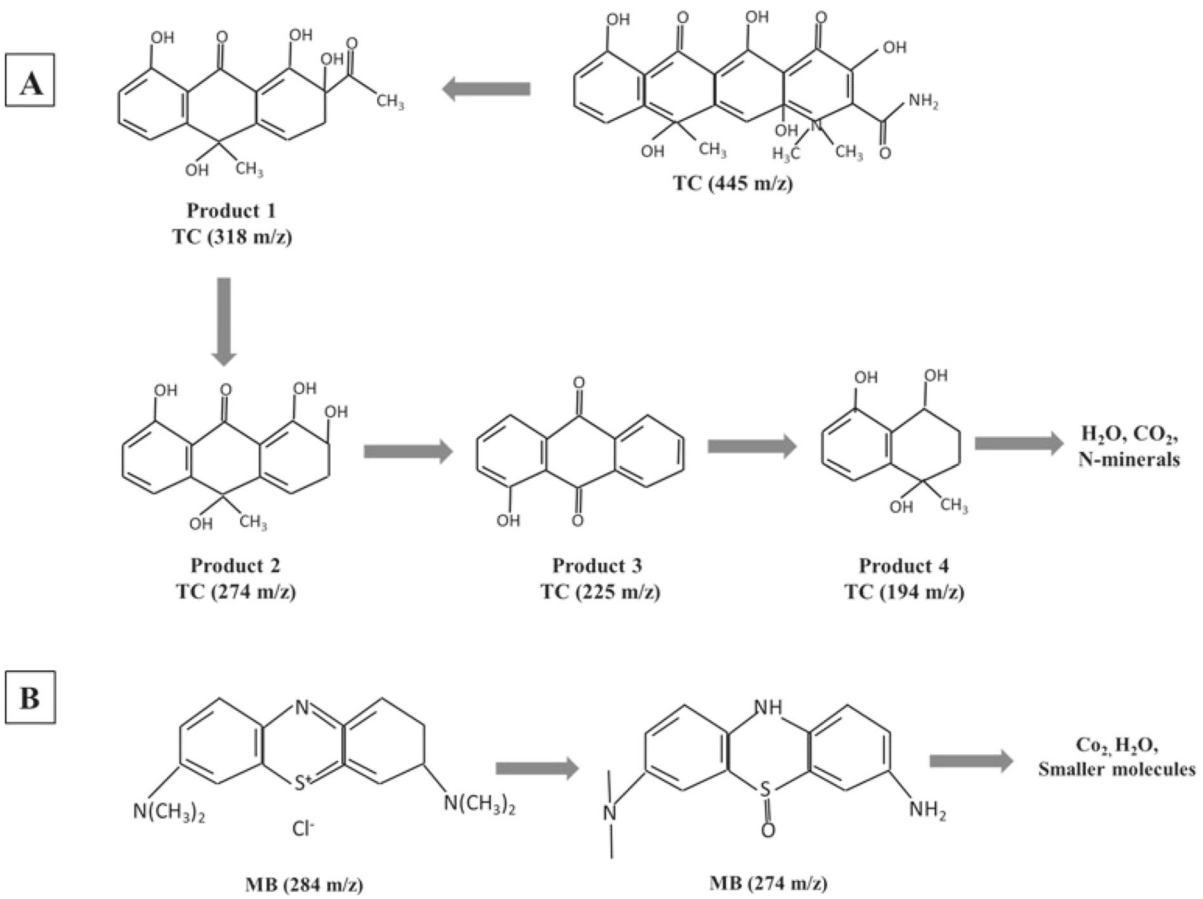

Fig. 8 The proposed degradation pathway for **A** Tetracycline **B** Methylene Blue

However, the byproducts formed via the decomposition of TC and MB are non-harmful to the environment. It is worth noting that 1.0 μm-sized rough particles were chosen for the study as they showed 100% removal efficiency in both semi-batch and batch conditions at a concentration of 100 ppm.

3.4 Kinetics of MB removal

Besides % of elimination, the order of the reaction and rate constant also provide good insight into the kinetics of the Pt-PS-assisted reactions. Langmuir-Hinshelwood (LH) kinetics is the most popular model for describing the kinetics of heterogeneous catalytic processes, which is described as shown in Eq. 1 below [42],

$$r = -\frac{dC}{dt} = \frac{k_r K C}{1 + K C} \tag{1}$$

Where r, k_r, K, and C refer to the rate of reaction that changes with time, limiting rate constant of reaction at maximum coverage under the given experimental conditions, the equilibrium constant for adsorption of the substrate onto the catalyst, and concentration at anytime t during degradation, respectively.

Most of the time, researchers approximated Eq. 1 to the first order, i.e., $n = 1$, by assuming $KC << 1$. Thus, when $-\mathbf{ln}\left(\frac{C}{C_0}\right)$ is plotted on the ordinate and time is plotted on the abscissa, the slope of the straight line is the product of k_r and K. However, if the value of the slope found is $>> 1$, then the assumption that $KC << 1$ becomes invalid. That means the subsequent kinetics will be in zero order. Figure 9 displays the pseudo-first-order kinetics corresponding to the heterogeneous reactions catalyzed by the rough particles of varying sizes. The rate constants for the reaction catalyzed by 0.6 and 1.0 μm particles at 50 ppm are 0.048 and 0.032 min^{-1}, respectively. The reported values are in the same order as that of the performance of the Fe-Pt nanoparticles reported by Hsieh and Lin for 5 ppm [5]. Due to variations in the concentration of the rough particles, the reported values in our case are 1.4 to 2.0 times higher than the literature value [5]. It is also noteworthy that the process catalyzed by the rough particles at a concentration of 50 ppm completes (100%) at the end of the 40-minute reaction time. By 90 minutes, the absorbance maximum near 665 nm for the Fe-Pt particles exhibited by Hsieh and Lin had dropped by just 90 % [5].

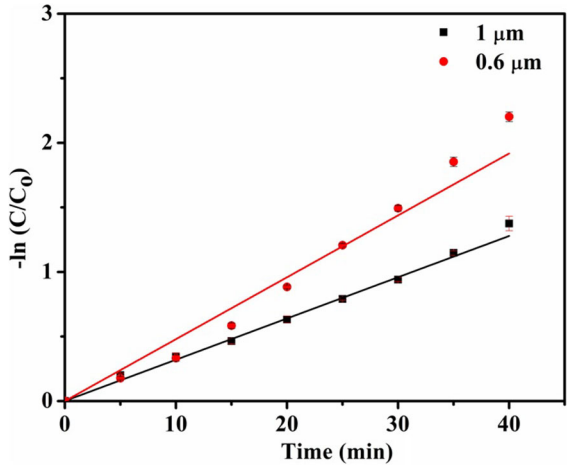

Fig. 9 Plot showing the pseudo-first-order kinetic study of MB degradation using rough particles of sizes 0.6 and 1.0 μm

Before moving on to the following section and exhibiting the proof-of-concept employing magnetically responsive particles, we propose probable causes for the disparity in performance between the different-sized rough particles. It is generally understood that the nanoparticles offer a more significant surface area (SA) for a given concentration in a batch reactor. For instance, we anticipate that the smaller rough particles would expose Pt significantly due to more particles than the same concentration of bigger rough particles. To account for any variations in the quality of Pt deposition, we refer to Table 1 for zeta potential values, AFM (Fig. 2), and electron mapping analysis (Fig. 2) of the rough particles of varying sizes. Based on these data, we assume that the quality of Pt deposition is consistent across all rough particle sizes. Consequently, the SA of rough particles should increase as their size decreases, i.e., 1.0 μm < 0.6 μm < 0.02 μm. In contrast, according to Figs. 7 and 9, we observed a kinetics that is an inverse function of particle size when examining the decomposition of MB using the rough particles under batch conditions. This unusual behaviour could be attributed to the crowding effect of bubbles and the buoyancy effect of the nanoparticles caused due to the attachment of bubbles. As a result, 1) particles diffuse rapidly towards the interface, decreasing the contact time with a key reactant, and 2) the catalyst's power is diminished due to a layer of bubbles around the particles obstructing the active sites. Figure 10 displays

the peroxide decomposition reaction as a function of time in minutes. Except for 0.6 and 1.0 μm, we found a marked difference in performance concerning 0.02 μm. The differences in peroxide breakdown kinetics found using the detector strips could be linked to the aforementioned factors. The video showing the rapid generation of the bubbles and the movement of the nanoparticles from bulk to the interface can be found in the supplementary information (Please see supplementary video-1 given in the supplementary information). Further, a gravimetric analysis has been performed to ensure that the catalytic activity reported is consistent with the degree of Pt loading per the rough particles of different sizes. The percentage loading was determined by measuring the mass of the bare and Pt-loaded PS particles at a known concentration of 100 ppm, as given in Eq. 2. The catalytic activity was calculated based on the performance of the rough particles at a specific decomposition time. For instance, the catalytic activity of the rough particles of sizes 0.02, 0.6, and 1 μm, obtained by deducing the percentage decomposition of MB at 10 min, are 2%, 95%, and 97%, respectively. Figure 11 displays the catalytic activity and Pt loading for the rough particles of varying sizes, with a particle concentration of 100 ppm, during the degradation of MB at a reaction time of 10 min using 5% H_2O_2. Figure 11 clearly illustrates that the smaller particles (0.02 μm) exhibit a higher Pt loading due to their larger surface area. However, their catalytic activity is significantly reduced due to the substantial generation of bubbles during H_2O_2 degradation and the buoyancy effect caused by the attachment of these bubbles and the rapid diffusion of nanoparticles toward the liquid-gas interface, as mentioned above.

$$\%Pt\ loading = ((Mass\ of\ catalyst)/(Mass\ of\ the\ bare\ PS)) \times 100 \quad (2)$$

3.5 Proof-of-concept

Thus far, we have demonstrated a straightforward methodology to make the rough particles by modifying the surface of the PS using the Pt nanoparticles through the wet-chemical route and their performances in decontamination application. Here, we show that the magnetically responsive rough particles (MR-RP) can be made by decorating platinum-coated PS nanoparticles with iron oxide nanoparticles like a core-shell structure to accomplish chemical deactivation and particle recovery in a single step. The benefits of MR-RP include ease of fabrication of Pt nanoparticles as the deposition takes place by attractive electrostatic forces between the Pt precursor (negatively charged) and the positively charged PS particles. This combination helps us achieve a uniform deposition like a monolayer of islands distributed throughout space without stabilizers like oleic acid and oleyl amine. Secondly, unlike the method proposed by Hsieh and Lin [5], the technique does not demand heating at high temperature, i.e., 297°C, and the entire process can be completed in room temperature.

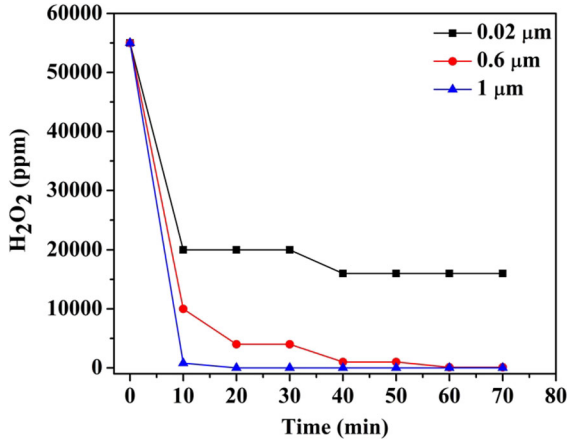

Fig. 10 H_2O_2 decomposition using the rough particles of varying sizes

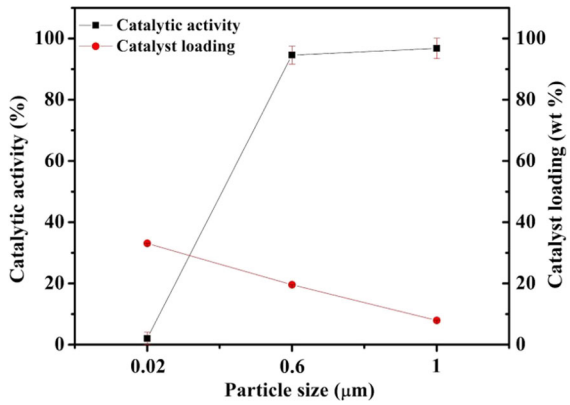

Fig. 11 Catalytic activity and loading versus a particular size of the rough particles

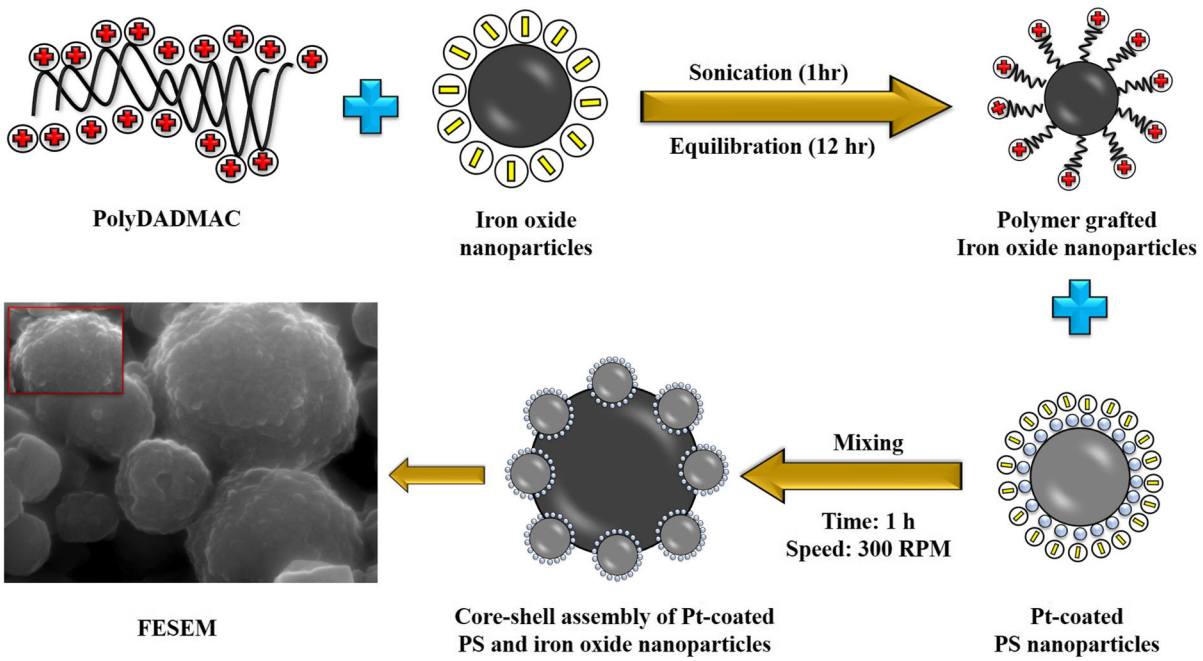

Fig. 12 Schematic description showing the process of synthesizing magnetically responsive rough particles using the wet-chemical method

To this end, we demonstrate the discolourization of MB using MR-RP. Figure 12 describes the process of making MR-RP using a wet-chemical route. Since the process follows the modifications in bulk, we can eliminate the shortcomings such as scale-up and yield. As shown in Fig. 12, the attractive forces between IO and Polydiallyldimethylammonium chloride (PolyDADMAC) allow the binding of the polymers on the surface of IO nanoparticles. Subsequently, the suspension containing Pt-modified PS nanoparticles of size 0.02 μm was introduced into the polymer-coated IO mixture. This addition results in the self-assembly of negatively charged Pt-modified PS and positively charged polymer-modified IO leading to the formation of core-shell particles. Note: Since the sufficient concentration of PS nanoparticles was considered during the wet-chemical deposition and a suitable ratio of Pt-decorated PS and polymer-decorated IO was chosen before mixing, there were very little or no free Pt nanoparticles found in the supernatant solution (Please see supplementary video-2 given in the supplementary information). We demonstrate a start-to-finish proof-of-concept of a two-step process (removal of MB + recovery of MR-RP) achieved by the proposed surface-engineered nanoparticles via a real-time video (Please see supplementary video-3 given in the supplementary information).

4 General remarks

We comment on the proposed method's applicability and shortcomings in this section. The proposed method works well against pollutants that accept electrons for

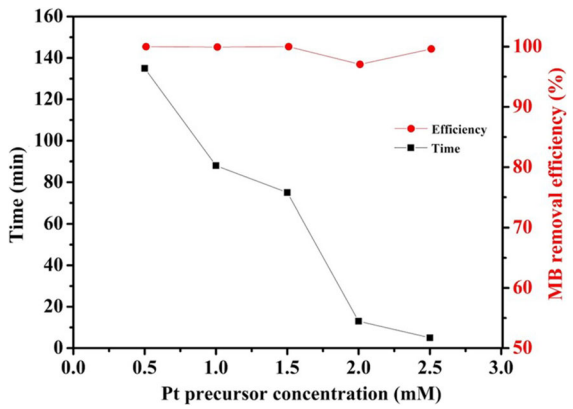

Fig. 13 MB degradation using platinum nanoparticles with 5% H_2O_2 in the batch mode

chemical deactivation. For instance, the process would not fit well for the methyl orange dye, a contaminant that would give up electrons while decomposing. The applicability of the rough particles was tested against methyl orange, and the decomposition rate is relatively slow compared to the reaction of its counterparts. Thus, we understand that the proposed rough particles show catalytic power and facilitate electron transfer from free radicals to pollutants over time. Secondly, the proposed method requires PS particles to be positively charged to attract the precursor ions, which are negatively charged, and induce nucleation of platinum nanoparticles on the surface of PS. Therefore, the method is unsuitable for making rough particles if the terminal end groups of PS are negatively charged. Our proposed methodology employs chloroplatinic acid (H_2PtCl_6) and research-grade polystyrene microspheres to establish a proof-of-concept. However, in practical large-scale applications, we can utilize nanoparticles derived from expanded polystyrene (EPS) waste through nanoprecipitation or green recycling methods, as reported in the literature [43–45]. Based on the stoichiometric analysis, treating one tonne of wastewater containing methylene blue (MB) as the target contaminant requires 10 g of platinum nanoparticles, assuming a rough particle concentration of 50 ppm. The calculated cost, including $NaBH_4$, is approximately $6200, based on analytical-grade quality. It is crucial to emphasize that there is substantial room for cost reduction, possibly by 10–20 times, with more cost-efficient sources in place of research-grade raw materials. The utilization of Pt nanoparticles in wastewater treatment encounters various challenges, including issues with separation and synthesis. A significant drawback is the prolonged degradation times observed for pollutants like MB. Figure 13 illustrates that the degradation time remains considerable despite achieving nearly 100% degradation of MB dye with Pt nanoparticles synthesized from different precursor solutions. Furthermore, increasing the nanoparticle concentration accelerates the degradation process, reducing the time required. However, when employing the same precursor quantity for synthesizing rough platinum particles, the resulting Pt-decorated PS particles exhibit swift and efficient degradation of pollutants. For instance, the synthesized platinum nanoparticles achieve complete degradation (100%) within 135 minutes, whereas the rough particles achieve an impressive 97% degradation within 10 minutes using the identical precursor quantity. The considerable variation in performance could be linked to a lack of active sites due to the depletion of catalytic activity associated with platinum-bubble collision and the buoyancy effect caused by the attachment of these bubbles.

5 Conclusion

We established a facile approach for producing Pt-studded PS-based rough particles with good catalytic activity in a single step. The proposed method offers an exciting route to make catalyst particles on desired supports at room temperature, compared to the existing process, which requires chemical precipitation followed by heating the reaction mixture to 297°C. Furthermore, the proposed approach could be an excellent alternative to existing Fenton-based heterogeneous particles studded with Pt metal nanoparticles. Our study revealed that the contacting patterns play a significant role in determining the performance of the rough particles over the decomposition of any given pollutant. For instance, the highest catalytic activity of PS-Pt rough particles was observed when tetracycline decomposition was performed in semi-batch rather than batch settings. Conversely, batch-wise operations recorded the maximal output of rough particles in eliminating methylene blue. Further, the impact of particle sizes, concentrations and dosing rate of hydrogen peroxide on the catalytic activity of rough particles was studied. To cite an example, the desired operating parameters to achieve 100% efficiency vary for different rough particles of size 0.6 μm (Optimum concentration = 200 ppm, dosing volume = 0.416 mL) and 1μm (Optimum concentration = 100 ppm, dosing volume = 1.25 mL). The heterogeneous reaction modelled by Langmuir-Hinshelwood kinetics indicates that the catalytic reaction follows the pseudo-first-order process with rate constants of 0.048 and 0.032 min^{-1} for the reaction catalyzed by 0.6 and 1.0 μm-sized rough particles, respectively. Using a well-known layer-by-layer technique, we presented a straightforward methodology to achieve a core-shell assembly of magnetically responsive rough particles (MR-RP). In a batch reactor configuration, the proof-of-concept for the decomposition of methylene blue using MR-RP was demonstrated. Since we can deactivate pollutants and recover catalyst particles in a single cycle, the proposed technique would be effective in real-time and large-scale applications

without incurring operating expenses. The study utilizing these rough particles in mitigating a target pollutant at various fluid-fluid interfaces is ongoing.

Acknowledgements We thank Dr. Neethu Thomas (Postdoctoral Researcher) and Prof. Parasuraman Swaminathan, Department of Metallurgical and Materials Engineering, IIT Madras, India, for helping us with the FESEM combined with the EDX analysis of our samples. We thank Mr Harsimranjit Singh, CRF, IIT Ropar, for helping us with the AFM imaging. The use of the BET facility at the Indian Institute of Technology Delhi (IIT Delhi) is greatly acknowledged. We are grateful for the insightful discussions on water quality analysis with Dr Vijay Anand from the Department of Civil Engineering at IIT Ropar. MS thanks IIT Ropar for providing the necessary funding assistance through a seed grant (ISIRD phase II) to set up a laboratory.

Funding Not applicable

Data Availibility The data sets produced during or analyzed during the current study are available from the corresponding author on reasonable request.

Compliance with ethical standards

Conflict of interest The authors declare no competing interests.

References

1. Visa M, Chelaru A-M (2014) Hydrothermally modified fly ash for heavy metals and dyes removal in advanced wastewater treatment. Appl Surf Sci 303:14–22
2. Liu L, Chen Z, Zhang J, Shan D, Wu Y, Bai L, Wang B (2021) Treatment of industrial dye wastewater and pharmaceutical residue wastewater by advanced oxidation processes and its combination with nanocatalysts: a review. J Water Proc Eng 42:102122
3. Peter A, Mihaly-Cozmuta A, Nicula C, Mihaly-Cozmuta L, Jastrzębska A, Olszyna A, Baia L (2017) UV light-assisted degradation of methyl orange, methylene blue, phenol, salicylic acid, and rhodamine b: photolysis versus photocatalyis. Water Air Soil Pollut 228(1):1–12
4. Mohammed HA, Khaleefa SA, Basheer MI (2021) Photolysis of methylene blue dye using an advanced oxidation process (ultraviolet light and hydrogen peroxide). Journal of Engineering and Sustainable Development 25(1)
5. Hsieh S, Lin P-Y (2012) FePt nanoparticles as heterogeneous Fenton-like catalysts for hydrogen peroxide decomposition and the decolorization of methylene blue. J Nanopart Res 14(6):1–10
6. Saleh R, Taufik A (2019) Degradation of methylene blue and congo-red dyes using Fenton, photo-Fenton, sono-Fenton, and sonophoto-Fenton methods in the presence of iron (II, III) oxide/zinc oxide/graphene (Fe3O4/ZnO/graphene) composites. Sep Purif Technol 210:563–573
7. Kirchon A, Zhang P, Li J, Joseph EA, Chen W, Zhou H-C (2020) Effect of isomorphic metal substitution on the Fenton and photo-Fenton degradation of methylene blue using Fe-based metal-organic frameworks. ACS Appl Mater Interfaces 12(8):9292–9299
8. Ikhlaqa A, Javedb F, Niaza A, Munirc HMS, Qid F (2020) Combined UV catalytic ozonation process on iron loaded peanut shell ash for the removal of methylene blue from aqueous solution. Desalin Water Treat 200:231–240
9. Xu Y, Yang S, Ying M, Lin X, Pan H (2023) Enhanced photocatalytic activity of Ag/ZnO@ ZIF-C with core-shell structure and multiple catalytic sites. Colloids Surf A 658: 130686
10. Lu J, Wang Y, Li H, Hu W, Zhou G, Sun B, Gu S (2023) Bi2mosxo6-x/α-cos crystalline/amorphous s-scheme heterojunction for visible light-driven targeted photo-decomposition of amoxicillin. Chem Eng J 144294
11. Adelin M, Gunawan G, Nur M, Haris A, Widodo D, Suyati L (2020) Ozonation of methylene blue and its fate study using LC-MS/MS. In: Journal of Physics: Conference Series, vol 1524. IOP Publishing, p 012079
12. Qian L-L, Blatov VA, Wang Z-X, Ding J-G, Zhu L-M, Li K, Li B-L, Wu B (2019) Sonochemical synthesis and characterization of four nanostructural nickel coordination polymers and photocatalytic degradation of methylene blue. Ultrason Sonochem 56:213–228
13. Dai X, Rao J, Bao Z, Li K, Feng L, Song D, Zhao L, Li W, Liu X, Yi S et al (2022) Magnetic double-core@ shell MnO2@ NiFe@ de as a multifunctional scavenger for efficient removal of tetracycline, anionic and cationic dyes. J Colloid Interface Sci 628:769–783
14. Dai X, Yi W, Yin C, Li K, Feng L, Zhou Q, Yi Z, Zhang X, Wang Y, Yu Y et al (2022) 2D–3D magnetic NiFe layered double hydroxide decorated diatomite as multi-function material for anionic, cationic dyes, arsenate, and arsenite adsorption. Appl Clay Sci 229:106664
15. Dai X, Jing C, Li K, Zhang X, Song D, Feng L, Liu X, Ding H, Ran H, Zhu K et al (2023) Enhanced bifunctional adsorption of anionic and cationic pollutants by MgAl LDH nanosheets modified montmorillonite via acid-salt activation. Appl Clay Sci 233:106815
16. Wang G, Xiang J, Lin J, Xiang L, Chen S, Yan B, Fan H, Zhang S, Shi X (2020) Sustainable advanced Fenton-like catalysts based on mussel-inspired magnetic cellulose nanocomposites to effectively remove organic dyes and antibiotics. ACS Appl Mater Interfaces 12(46):51952–51959
17. Lin J, Chen S, Xiao H, Zhang J, Lan J, Yan B, Zeng H (2020) Ultra-efficient and stable heterogeneous iron-based Fenton nanocatalysts for degrading organic dyes at neutral pH via a chelating effect under nanoconfinement. Chem Commun 56(48):6571–6574
18. Xia H, Li C, Yang G, Shi Z, Jin C, He W, Xu J, Li G (2022) A review of microwave-assisted advanced oxidation processes for wastewater treatment. Chemosphere 287:131981
19. Wang D, Hu Y, Cui Z, Yang P, Du Z, Hou Y, Yang P, Rao J, Wang C, Zhang Y (2023) Sulfur vacancy regulation and multipolarization of nixco1s nanowires-decorated biotemplated structures to promote microwave absorption. J Colloid Interface Sci 646:991–1001
20. Wang D, Yang P, Hu Y, Cui Z, Du Z, Yang P, Yi S, Rao J, Zhang Y (2023) 1D–3D biological template loaded NiCo nanowires at high temperatures as a broadband, lightweight

electromagnetic wave absorbing material. Powder Technol 426:118670
21. Zhang C, Wang D, Dong L, Li K, Zhang Y, Yang P, Yi S, Dai X, Yin C, Du Z et al (2022) Microwave absorption of α-Fe2O3@ diatomite composites. Int J Mol Sci 23(16):9362
22. Du Z, Wang D, Zhang X, Yi Z, Tang J, Yang P, Cai R, Yi S, Rao J, Zhang Y (2022) Core-shell structured SiO2@ NiFe LDH composite for broadband electromagnetic wave absorption. Int J Mol Sci 24(1):504
23. Liu Y, He X, Fu Y, Dionysiou DD (2016) Degradation kinetics and mechanism of oxytetracycline by hydroxyl radical-based advanced oxidation processes. Chem Eng J 284:1317–1327
24. Pignatello JJ, Oliveros E, MacKay A (2006) Advanced oxidation processes for organic contaminant destruction based on the Fenton reaction and related chemistry. Crit Rev Environ Sci Technol 36(1):1–84
25. Giordano G, Perathoner S, Centi G, De Rosa S, Granato T, Katovic A, Siciliano A, Tagarelli A, Tripicchio F (2007) Wet hydrogen peroxide catalytic oxidation of olive oil mill wastewaters using Cu-zeolite and Cu-pillared clay catalysts. Catal Today 124(3):240–246. https://doi.org/10.1016/j.cattod.2007.03.041. Advanced Catalytic Oxidation Processes
26. Ai Z, Lu L, Li J, Zhang L, Qiu J, Wu M (2007) Fe@ Fe2O3 core- shell nanowires as iron reagent. 1. Efficient degradation of rhodamine B by a novel sono-Fenton process. J Phys Chem C 111(11):4087–4093
27. Toda T, Igarashi H, Uchida H, Watanabe M (1999) Enhancement of the electroreduction of oxygen on Pt alloys with Fe, Ni, and Co. J Electrochem Soc 146(10):3750–3756. https://doi.org/10.1149/1.1392544
28. Dokoutchaev A, James JT, Koene SC, Pathak S, Prakash GS, Thompson ME (1999) Colloidal metal deposition onto functionalized polystyrene microspheres. Chem Mater 11(9):2389–2399
29. Lee J-H, Mahmoud MA, Sitterle V, Sitterle J, Meredith JC (2009) Facile preparation of highly-scattering metal nanoparticle-coated polymer microbeads and their surface plasmon resonance. J Am Chem Soc 131(14):5048–5049
30. Bao H, Bihr T, Smith A-S, Taylor RNK (2014) Facile colloidal coating of polystyrene nanospheres with tunable gold dendritic patches. Nanoscale 6(8):3954–3966
31. Wang D-S, Mukhtar A, Wu K-M, Gu L, Cao X (2019) Multi-segmented nanowires: a high tech bright future. Materials 12(23):3908
32. Wang D, Mukhtar A, Humayun M, Wu K, Du Z, Wang S, Zhang Y (2022) A critical review on nanowire-motors: design, mechanism and applications. Chem Rec 22(8):202200016
33. Sabapathy M, Kollabattula V, Basavaraj MG, Mani E (2015) Visualization of the equilibrium position of colloidal particles at fluid-water interfaces by deposition of nanoparticles. Nanoscale 7(33):13868–13876
34. Lu L, Sun G, Xi S, Wang H, Zhang H, Wang T, Zhou X (2003) A colloidal templating method to hollow bimetallic nanostructures. Langmuir 19(7):3074–3077
35. Karimi S, Moshaii A, Nikkhah M (2019) Controlled synthesis of colloidal monodisperse gold nanoparticles in a wide range of sizes; investigating the effect of reducing agent. Mater Res Express 6(11):1150–1152
36. Mikhlin Y, Karacharov A, Likhatski M, Podlipskaya T, Zubavichus Y, Veligzhanin A, Zaikovski V (2011) Submicrometer intermediates in the citrate synthesis of gold nanoparticles: new insights into the nucleation and crystal growth mechanisms. J Colloid Interface Sci 362(2):330–336
37. Hansen HE, Seland F, Sunde S, Burheim OS, Pollet BG (2021) Two routes for sonochemical synthesis of platinum nanoparticles with narrow size distribution. Mater Adv 2(6):1962–1971
38. Dubber D, Gray NF (2010) Replacement of chemical oxygen demand (COD) with total organic carbon (TOC) for monitoring wastewater treatment performance to minimize disposal of toxic analytical waste. J Environ Sci Health A 45(12):1595–1600
39. Yang Y, Zeng Z, Zhang C, Huang D, Zeng G, Xiao R, Lai C, Zhou C, Guo H, Xue W et al (2018) Construction of iodine vacancy-rich BiOI/Ag@ AgI z-scheme heterojunction photocatalysts for visible-light-driven tetracycline degradation: transformation pathways and mechanism insight. Chem Eng J 349:808–821
40. Fang S, Zhang W, Sun K, Hu YH (2022) Highly efficient thermo-photocatalytic degradation of tetracycline catalyzed by tungsten disulfide under visible light. Environ Chem Lett 1–9
41. Wang H, Zhou P, Guo R, Wang Y, Zhan H, Yuan Y (2018) Synthesis of rectorite/Fe3O4/ZnO composites and their application for the removal of methylene blue dye. Catalysts 8(3):107
42. Kumar KV, Porkodi K, Rocha F (2008) Langmuir-hinshelwood kinetics - a theoretical study. Catal Commun 9(1):82–84. https://doi.org/10.1016/j.catcom.2007.05.019
43. Rajeev A, Erapalapati V, Madhavan N, Basavaraj MG (2016) Conversion of expanded polystyrene waste to nanoparticles via nanoprecipitation. J Appl Polym Sci 133(4)
44. Mangalara SCH, Varughese S (2016) Green recycling approach to obtain nano-and microparticles from expanded polystyrene waste. ACS Sustain Chem Eng 4(11):6095–6100
45. Pawak VS, Shekhar C, Loganathan VA, Sabapathy M (2023) Separation of nanoplastics from synthetic and industrial wastewater using electrolysis-assisted flotation approach: a green approach for real-time contaminant mitigation. Chem Eng Res Des 198:184–195